Res Chem Intermed (2018) 44:2667–2683
https://doi.org/10.1007/s11164-018-3253-z

Synthesis of Fe- or Ag-doped TiO_2–MWCNT nanocomposite thin films and their visible-light-induced catalysis of dye degradation and antibacterial activity

Md. Asjad Hossain[1,2] · Md. Elias[1,3] · Dali Rani Sarker[1] · Zidnia Rahman Diba[1] · Jannatul Morshed Mithun[1] · Md Abul Kalam Azad[4] · Iqbal Ahmed Siddiquey[1] · Mohammed M. Rahman[5] · Jamal Uddin[6] · Md. Nizam Uddin[1]

Received: 6 September 2017 / Accepted: 8 January 2018 / Published online: 18 January 2018

Abstract Thin films of TiO_2, TiO_2-multiwalled carbon nanotubes (TiO_2–MWCNT), Fe-doped TiO_2–MWCNT (Fe–TiO_2–MWCNT), and Ag-doped TiO_2–MWCNT (Ag–TiO_2–MWCNT) supported on glass substrates were successfully prepared by sol–gel drop coating method. MWCNTs were treated by H_2SO_4 and HNO_3 to oxidize graphitic carbon. The composites were characterized by scanning electron microscopy (SEM), X-ray diffraction (XRD) analysis, Fourier-transform infrared (FTIR) spectroscopy, and ultraviolet–visible (UV-Vis) absorption spectroscopy to confirm their structure and optical properties. XRD patterns of all prepared films exhibited (101), (004), (200), (105), (211), (204), (116), (220), (215), and (224) planes of anatase-phase TiO_2. A pronounced broad peak at ~3400 cm^{-1} in the FTIR spectrum of the MWCNT confirmed oxidation of some carbon atoms on the surface of MWCNTs by HNO_3 and H_2SO_4. The photocatalytic and antibacterial activities of

Md. Asjad Hossain and Md. Elias contributed equally to this work.

✉ Md. Nizam Uddin
nizam3472@yahoo.com

[1] Department of Chemistry, Shahjalal University of Science and Technology, Sylhet 3114, Bangladesh

[2] Department of Chemistry, University of Alberta, Edmonton, AB T6G 2G2, Canada

[3] Department of Chemistry, Jagannath University, Dhaka 1100, Bangladesh

[4] Department of Genetic Engineering and Biotechnology, Shahjalal University of Science and Technology, Sylhet 3114, Bangladesh

[5] Chemistry Department, Faculty of Science and Center of Excellence for Advanced Materials Research, Kind Abdulaziz University, Jeddah, Saudi Arabia

[6] Department of Natural Sciences, Coppin State University, Baltimore, MD 21216, USA

the prepared materials were tested under visible-light irradiation based on degradation of methylene blue (MB) dye in aqueous solution and reduction in the viable count of *Escherichia coli*, respectively. Fe or Ag was doped into the TiO_2-MWCNT composites, lowering the bandgap and thereby enabling enhanced photocatalytic activity in the visible-light region. Based on the MB photodegradation results, the photocatalytic efficiency of the Fe–TiO_2–MWCNT and Ag–TiO_2–MWCNT composites could be due to the following mechanism: (1) adsorption and photoinduced electron absorption by MWCNT, and (2) electron trapping by Fe or Ag within the TiO_2 matrix, in addition to the usual photocatalytic activity of TiO_2. Moreover, as-synthesized Ag–TiO_2–MWCNT composite films showed outstanding antimicrobial activity.

Keywords Nanocomposite · Antibacterial activity · Thin films · Catalysis · Photocatalytic activity

Introduction

In recent years, extensive research has been conducted on heterogeneous photocatalysts. Titanium dioxide (TiO_2) is one of the most commonly used photocatalysts because of its low cost, nontoxicity, chemical stability, and resistance to chemical corrosion and optical degradation [1–4]. It is a wide-bandgap (3.2 eV) semiconductor and excellent photocatalyst for degradation of a wide variety of organic and inorganic substances [5]. Its capability for nonselective and complete mineralization of dye pollutants has also been demonstrated, being due to production of hydroxyl radicals ($OH^{\cdot}$) and superoxide anions ($O_2^{\cdot -}$) when TiO_2 absorbs UV radiation while in contact with water and oxygen, according to the following widely accepted mechanism [6]:

(a) Absorption of effective photons ($h\nu \geq E_g = 3.2$ eV) by TiO_2

$$TiO_2 + h\nu \rightarrow h_{vb}^{+} + e^{-}$$

(b) Generation of $O_2^{\cdot -}$ and $OH^{\cdot}$ by electron–hole pairs

$$H_2O + h_{vb}^{+} \rightarrow H^{+} + OH^{\cdot}$$

$$\left(O_2\right)_{ads} + e^{-} \rightarrow O_2^{\cdot -}$$

(c) Oxidation of the organic reactant by successive attack by $OH^{\cdot}$ and $O_2^{\cdot -}$ radicals

$$Dye + OH^{\cdot} \rightarrow Dye^{*} + H_2O$$

$$Dye^{*} + h_{vb}^{+} \rightarrow Dye^{**} + CO_2$$

$$Dye + O_2^{\cdot -} \rightarrow Dye^{***}$$

where Dye*, Dye**, and Dye*** denoted successive breakdown products of the dye molecule. However, the photocatalytic efficiency of TiO_2 is low due to the high electron–hole recombination rate. Moreover, there are other drawbacks with use of suspended TiO_2 powders, for instance difficulties associated with separation of the catalyst from treated wastewater after each run [7]. Recently, various approaches have been proposed to amend these difficulties; For example, TiO_2 particles have been supported on different substrate materials [8–10] or transition-metal ions, namely Co, Ag, Pt, Ni, Ce, and Fe, have been incorporated [11–16].

Nanocomposites based on carbon nanotubes (CNTs) are better candidate materials that have attracted significant attention from researchers due to their ability to adhere to semiconducting nanomaterials, thereby preventing aggregation and inhibiting electron–hole recombination. A large variety of CNT-based photocatalytic materials such as TiO_2-CNT nanocomposites prepared by modified sol–gel methods have been reported recently [17, 18]. TiO_2 nanoparticles comodified with carbon and Fe were prepared by thermal treatment of precursors at 500–800 °C in argon atmosphere [19]. The resultant nanocomposites demonstrated notably enhanced photodegradation of dyes through a photo-Fenton process, where hydroxyl radicals are produced. It was reported that Ag-supported CNTs showed high electrocatalytic activity for hydrazine oxidation [20], indicating that Ag catalyst may be used to replace noble-metal catalysts such as Pt, Au, etc. [13, 21]. In addition, the high activity of silver-ion-modified titanium dioxide suspensions for mineralization of sucrose was mainly ascribed to presence of small silver particles on the titania surface, rather than to trapping of electrons during reduction of silver ions [22]. The enhanced reduction of oxygen through better electron–hole separation in Ag/TiO_2 particles compared with pure TiO_2 particles increases the rate of sucrose mineralization. Zhang et al. [23] also reported photoelectrocatalytic properties of Ag-CNT/TiO_2 composite electrodes for degradation of methylene blue (MB), in which presence of silver ions is believed to retard e^-/h^+ recombination by serving as an electron sink (Schottky-barrier electron trapping) and to facilitate interfacial electron transfer to dioxygen or other electron acceptors.

Recently, our group reported synthesis of a B/N-codoped TiO_2 composite that showed good photocatalytic performance for degradation of MB under visible light [7]. To the best of the authors' knowledge, Fe- or Ag-doped TiO_2–MWCNT composites have not been synthesized to date. Therefore, in this research, we focused on synthesis of Fe–TiO_2–MWCNT and Ag–TiO_2–MWCNT composite thin films using a sol–gel method and compared their photocatalytic efficiency under visible-light irradiation. The advantageous influence of the combination of each dopant and MWCNT in the TiO_2 structure was explored. The structural, morphological, and optical properties of the prepared samples were analyzed in detail. The antibacterial activity of the synthesized nanocomposites against *E. coli* bacteria was also explored.

Experimental

Materials

Titanium(IV) isopropoxide (TIP) (≥97.0 %, Sigma Aldrich) and triethylamine (TEA) (≥99 %, Sigma Aldrich) were used as TiO_2 source and stabilizer, respectively. Soda lime glass microscope slides (1″ × 3″) were used as substrate. Ferrous sulfate (99.5 %) and silver nitrate (99.8 %) (Merck, Germany) were used as Fe and Ag source. MB was purchased from Merck, Germany. All reagents were of analytical grade and used without further purification.

Visible-light chamber

The chamber consisted of a rectangular glass box with dimensions of 16″ × 10″ × 12″, with an upper open slide, which was covered by a removal hardboard. The inner side of the box and hardboard were covered with aluminum foil to maximize the light intensity. A water inlet and outlet were used to maintain cooling water flow. A visible-light source (200 W, tungsten lamp) was also applied on the cover for light irradiation in the box. The distance between the dye solution and visible lamp was 20 cm. The water flow was controlled by a pump. A schematic diagram of the reactor is shown in Fig. 1.

Functionalization of MWCNT

MWCNT (1.0 g) were immersed in 40 ml mixed solution of concentrated sulfuric acid and nitric acid with volume ratio of 1:1 [24]. The mixture was then refluxed at 70–80 °C for 5 h to obtain dark-brown suspension and cooled naturally to room temperature. The MWCNT were filtered and washed with distilled water until the pH of the filtered solution reached about 6–7. The product was then dried at 80 °C in a vacuum oven for 8 h and kept for further use.

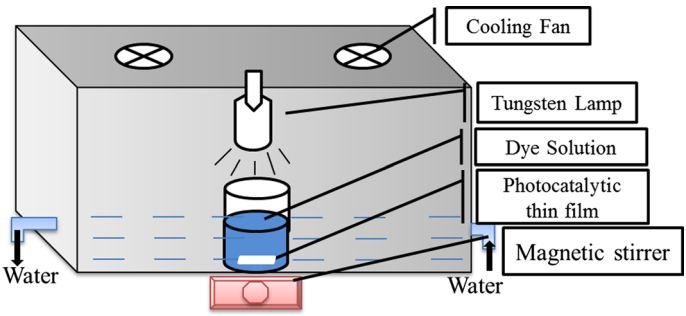

Fig. 1 Schematic diagram of visible-light degradation chamber

Fabrication of thin films

TiO_2 thin films were synthesized per previous procedure [7]. Briefly, 1.0 ml TIP was added to 6.67 ml anhydrous ethanol under vigorous stirring, then 0.24 ml TEA was added as stabilizer, followed by stirring at 200 rpm for 2–3 min (solution A). A second solution was prepared separately by mixing hydrochloric acid (0.60 ml), water (0.10 ml), and anhydrous ethanol (6.67 ml) using a magnetic stirrer at 200 rpm (solution B). The two solutions were then mixed dropwise and stirred vigorously for 60 min. The total volume of the solution was maintained at 16 ml by adding ethanol. The resulting TiO_2 sol was transparent, quite stable, and highly sensitive to the amount of TEA and water. The sol was then aged for 24 h and used for film preparation.

The transparent sol was usually stable for 3 weeks. TiO_2 thin films were prepared by drop coating method, in which the amount of coating material can easily be controlled within a fixed surface area, as well as the film thickness. Prior to the coating process, soda lime silica glass substrates (microscope slides) with dimensions of 10 mm × 60 mm × 1.5 mm were ground using a commercial bench grinder (model ST-150) followed by cleaning in potassium dichromate and dichloromethane solution. Finally, the abrasive substrates were rinsed with alcohol and distilled water, then dried at 100 °C.

TiO_2 gel films were obtained by coating an appropriate volume of precursor solution onto the glass. The coated substrates were pretreated at room temperature, then annealed for 20 min at 200 °C. Finally, the film was vapor treated in the vapor of boiling water for 30 s to remove loosely bonded particles. The coating process was repeated two times to prepare thick (~4 μm) film, followed by annealing at 500 °C for 2 h in a muffle furnace (JSMF-30T, Korea).

Thin films of TiO_2–MWCNT, Ag–TiO_2–MWCNT, and Fe–TiO_2–MWCNT were prepared using a similar method ("Fabrication of thin films" section) by separately dissolving 0.5 mg/ml MWCNT and 5 wt% ferrous sulfate or 5 wt% silver nitrate in anhydrous ethanol then rapidly adding to the mixture of solution A and solution B, respectively. These are denoted as CT, SCT, and FCT, respectively. Here, the total volume of solution was also maintained at 16 ml by addition of ethanol.

Characterization

Composite films based on TiO_2 were characterized using a range of analytical techniques. The morphology of the prepared films was investigated by scanning electron microscopy (SEM, JSM-7600F, Japan). XRD patterns were recorded using an X-ray diffractometer (XRD, D8 ADVANCE, Bruker, Germany) with Cu K_α radiation ($\lambda = 0.15418$ nm) at 40 kV and 40 mA over the 2θ range from 10° to 90° at room temperature. Fourier-transform infrared (FTIR) spectra of functionalized MWCNTs were recorded using a Shimadzu dxp 400 (Japan) from KBr disks of about 150 mg containing approximately 2 % sample prepared shortly before recording the spectra in the range from 400 to 4000 cm^{-1} at resolution of 4 cm^{-1}. UV–Vis spectra in the

wavelength range of 200–800 nm were obtained using a UV–Vis spectrophotometer (UV-1800, Shimadzu, Japan).

Photocatalytic studies

The photocatalytic activity of the films was studied using degradation of MB dye as a model pollutant in the visible-light chamber shown in Fig. 1. The TiO_2 thin films were placed in a beaker containing 200 ml 5×10^{-6} M MB, then irradiated by tungsten lamp. After irradiation for 30, 60, 90, 120, 150, 210, and 240 min, the residual concentration of MB was determined by UV–Vis spectrophotometer (UV-1800, Shimadzu, Japan). The photodegradation efficiency of the thin films was calculated as

$$\text{Efficiency}\,(\%) = (C_0 - C_t)/C_0 \times 100 = \left(A_0 - A_t\right)/A_0 \times 100, \tag{1}$$

where C_t and A_t are the concentration and absorbance at 664 nm of the MB solution after irradiation for time t, and C_0 and A_0 are the concentration and absorbance at 664 nm of the MB solution before irradiation. Kinetic models were employed to analyze the data obtained during photodegradation by the prepared samples.

The first-order model was used to analyze the data obtained during the first photodegradation cycle of the prepared catalytic thin films [25], generally expressed as

$$\log\left(C_t/C_0\right) = -kt, \tag{2}$$

where C_0 and C_t are the concentration of MB at irradiation time zero and t, respectively, and k is the first-order rate constant.

Antibacterial activity study

The antibacterial activity of all the composite thin films was investigated using the antibacterial drop-test method [26]. The size of all films used in this experiment was 25 mm × 25 mm. Diluted *E. coli* suspension (250 µl) prepared in physiological saline suspension was spread on the surface of each film followed by irradiation by tungsten lamp at room temperature. After 60 min, the bacteria were washed from the surface of the film using 16 mL sterile physiological saline into a sterilized conical flask. Then, 25 µl of each suspension was spread on a nutrient agar plate and incubated at 37 °C for 24 h to determine the viable bacterial count. The reported values are averages of three similar independent experiments.

Results and discussion

Morphology of photocatalytic thin films

SEM images showing the surface morphology of the bare-TiO_2, TiO_2–MWCNT (CT), Fe–TiO_2–MWCNT (FCT) and Ag-TiO_2-MWCNT (SCT) films are shown in Fig. 2. All the samples were annealed at 500 °C for 2 h. Significant cracking was observed on the surface of all films. The different types of cracking observed might

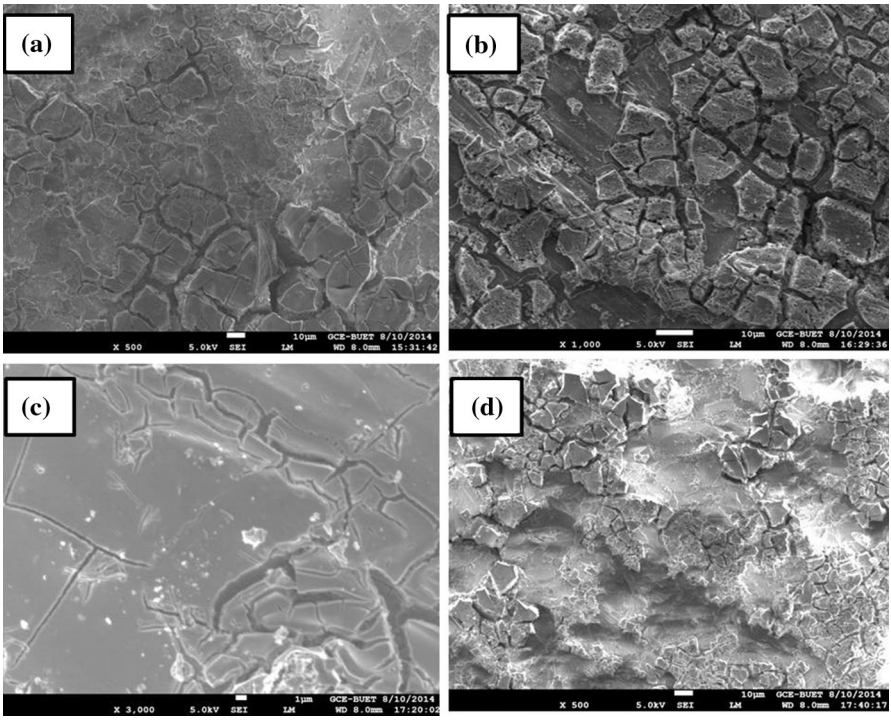

Fig. 2 SEM images of **a** bare-TiO_2, **b** CT, **c** FCT, and **d** SCT

be due to the different thermal expansion coefficient mismatch between bare-TiO_2, CT, FCT, and SCT versus the glass substrate. Such cracking might increase the surface area available for catalytic reaction. The morphology of the films is comparable to that of B/N-doped TiO_2 films prepared on glass substrate, as previously reported by our group [7]. The lack of observation of MWCNT by SEM may be due to their lower concentration compared with TiO_2. However, the presence of carbon and dopant atoms was observed by energy dispersive X-ray spectroscopy (EDS). A representative EDS spectrum is shown in Fig. 3, and the atomic percentage of each atom is summarized in Table 1. The higher amount of oxygen observed is due to the use of silica glass (SiO_2) as substrate.

XRD analysis

XRD patterns depicting the crystalline structure of bare TiO_2, CT, SCT, and FCT films are shown in Fig. 4. For the TiO_2 and composite catalysts, all the sharp peaks observed in the XRD patterns at 2θ = 24.6°, 36.9°, 47.2°, 52.4°, 53.7°, 61.1°, 66.8°, 68.6°, 73.6°, and 80.8° correspond to (101), (004), (200), (105), (211), (204), (116), (220), (215), and (224) planes of anatase-phase TiO_2, respectively. Note that the characteristic peaks of CNTs are barely observable in the patterns of all the

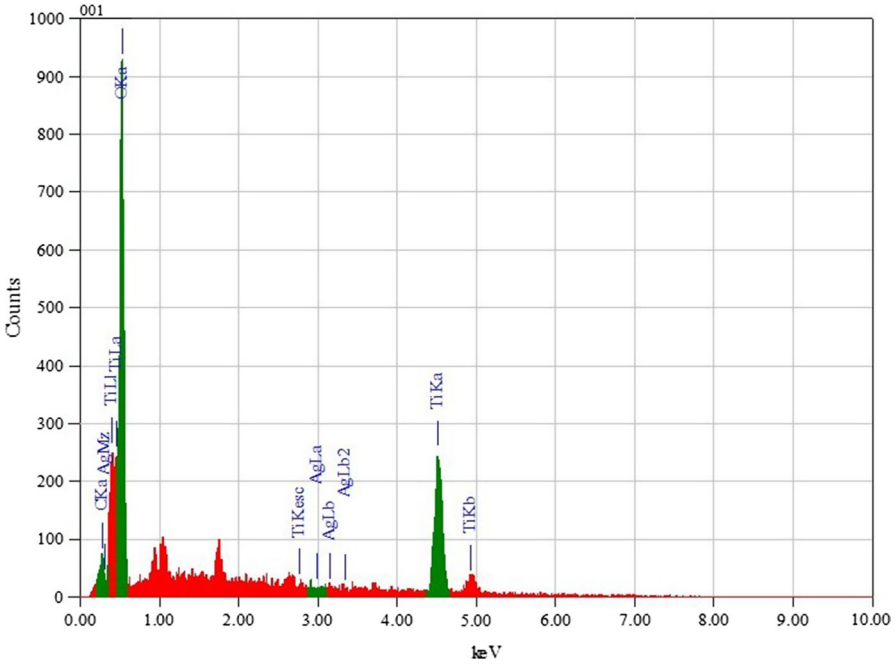

Fig. 3 EDS spectrum of Ag–TiO_2–MWCNT (SCT) thin film

Table 1 Elemental analysis of bare-TiO_2, CT, FCT, and SCT composite thin films

Sample	Ti (at.%)	O (at.%)	C (at.%)	Ag (at.%)	Fe (at.%)
Bare-TiO_2	11.32	88.68	–	–	–
CT	15.17	79.97	4.68	–	–
FCT	25.99	70.32	2.97		0.72
SCT	8.05	88.43	3.42	0.10	–

composite catalysts. This is due to the overlap between the main CNT peak at 25.9° with the main peak of anatase TiO_2 at 24.6° [27]. There was no observable shift in the XRD patterns among the bare TiO_2, CT, SCT, and FCT films. This may be due to the very small amount of doping of Ag and Fe, as shown in Table 1.

The mean crystallite size was calculated from the full-width at half-maxima of the (101) peak of anatase TiO_2 using the Debye–Scherrer formula:

$$D = \frac{K\lambda}{\beta\cos\theta},$$

where λ is the wavelength of Cu K_α irradiation ($\lambda = 0.15418$ nm), K is the Scherrer constant ($K = 0.89$), θ is the diffraction angle, and β is the full-width at half-maximum [28]. The calculated average crystallite size of the composites was 11.40,

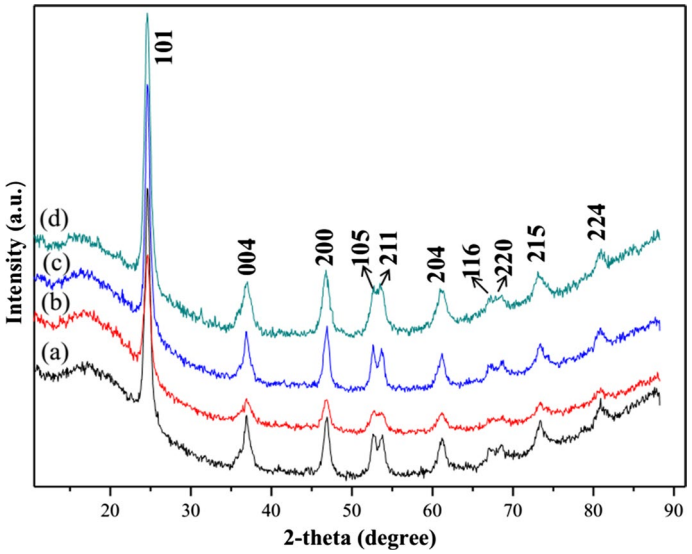

Fig. 4 XRD patterns of **a** bare-TiO_2, **b** CT, **c** FCT, and **d** SCT

11.01, 12.50, and 9.87 nm for TiO_2, CT, FCT, and SCT, respectively. The smaller crystallite size observed on silver ion doping can be explained by distortion of the crystal structure in the presence of the dopant. Santos et al. [29] observed the same phenomenon after silver ion doping. However, the presence of Fe species slightly increased the crystallite size, which was never been seen by previous researchers [30]. This anomalous observation is still under investigation in our current research. The XRD spectra did not exhibit any distinct reflections for silver or iron species, indicating good dispersion of the dopants in the TiO_2 [29].

FTIR analysis

Figure 5a, b show the FTIR spectra of pure and acid-treated functionalized MWCNT, respectively. The FTIR spectrum of pure MWCNT showed a weak broad peak at ~3400 cm^{-1}, corresponding to O–H stretching of moisture absorbed from the environment. The acid-treated MWCNT showed a pronounced broad peak at ~3400 cm^{-1} due to oxidation of some carbon atoms on the surfaces of the MWCNT by HNO_3 and H_2SO_4 [24]. The FTIR spectra of the composites are not shown because they provide no useful information other than broad Ti–O–Ti stretching below 1000 cm^{-1}.

UV–Vis absorption spectroscopy

Figure 6 compares the UV–Vis absorption spectra of thin films of bare-TiO_2, CT, FCT, and SCT. The absorption by the catalysts in the visible-light region increased

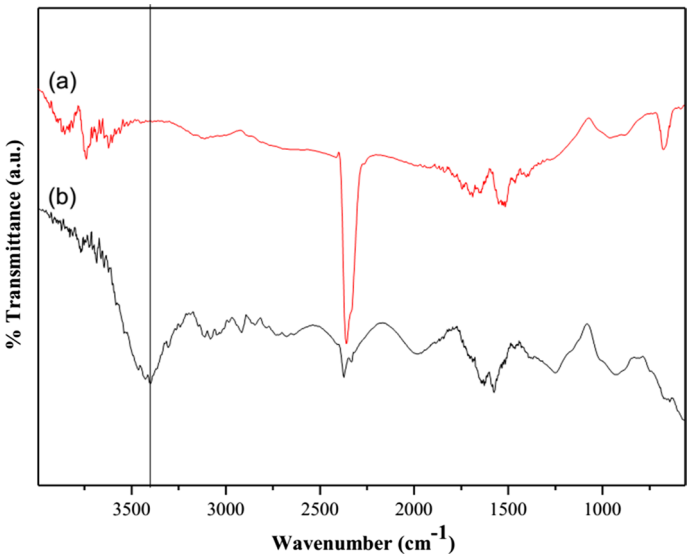

Fig. 5 FTIR spectra of **a** pure MWCNT, and **b** functionalized MWCNT

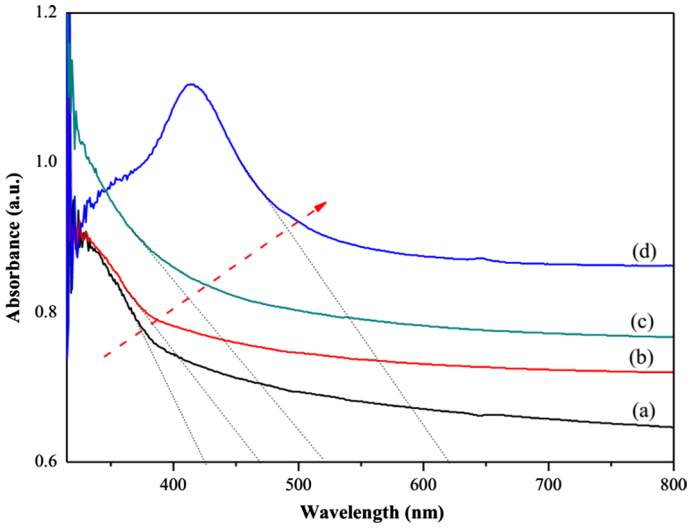

Fig. 6 UV–Vis absorption spectra of **a** TiO_2, **b** CT, **c** FCT, and **d** SCT thin films

after Fe or Ag doping, decreasing in the following order: SCT > FCT > CT > bare-TiO_2 in the wavelength range of 400–800 nm. This clear red-shift (indicated by the dotted arrow) in the absorption onset reveals narrowing of the bandgap of TiO_2 by Ag or Fe doping. The reason why the most intense peak was observed for SCT is

the surface plasmon resonance of silver [28]. Moreover, the red-shift observed after doping was significantly higher compared with that of CT or bare-TiO_2.

The general relationship between the bandgap energy E_g (eV) of TiO_2 and its wavelength λ (nm) is given by the following equation:

$$E_g = 1240/\lambda.$$

From the above equation, it follows that, the higher the wavelength of maximum absorption λ (nm), the narrower the bandgap E_g (eV). The estimated bandgap energy was 2.93, 2.67, 2.38, and 2.01 eV for TiO_2, CT, FCT, and SCT, respectively. This result indicates that incorporation of iron or silver dopant into titania caused a remarkable reduction in the bandgap energy that induced a red-shift of the photo-excitation response to the visible region. It is generally accepted that most transition-metal energy levels lie between the valance and conduction band of titania [5]. Therefore, an electronic transition from Fe^{3+} or Ag^+ energy levels to the conduction band of titania is considered to be the main reason for this reduction in the bandgap energy and shift of the absorption response to the visible-light region.

Photocatalytic activity

It is well known that MB is one of the most hazardous organic dyes present in wastewater, causing serious environmental problems. MB has already been recognized as a standard dye in the research field of photocatalysis. We therefore studied the photodegradation of this due under visible-light irradiation to evaluate the photocatalytic activity of the prepared catalysts. A typical representation of absorption behavior is shown in Fig. 7, displaying the changes in the absorbance profile of MB solution in presence of SCT under visible-light irradiation. The maximum absorption characteristic peak is observed at wavelength of 664 nm. The intensity of the peak reduced quickly with increasing duration of visible-light irradiation. Figure 8 shows the MB photodegradation efficiency of the prepared catalysts, with SCT exhibiting the highest photocatalytic activity under visible-light irradiation.

The kinetic rate constant (k, min^{-1}) was calculated and is presented in Fig. 9. The photocatalytic degradation of MB obeyed pseudo-first-order reaction kinetics [25].

Antibacterial activity

The antibacterial activity of the thin films was investigated against *E. coli*. The reduction in the viable count of *E. coli* on the nanocomposite thin films under visible-light irradiation is shown in Fig. 10.

It is clearly seen that the reduction of *E. coli* was very high in case of the Ag–TiO_2–MWCNT composite film compared with TiO_2. This may be due to various reactive oxygen species (O_2^-, OH^-, H_2O_2, etc.) generated on the photocatalyst by visible-light irradiation. Cell death of *E. coli* through breakdown of the cell membrane structure may occur due to lipid peroxidation under the influence of such reactive species [31]. Moreover, the antimicrobial properties of silver compounds and silver ions have been historically recognized and used in a wide range of applications for

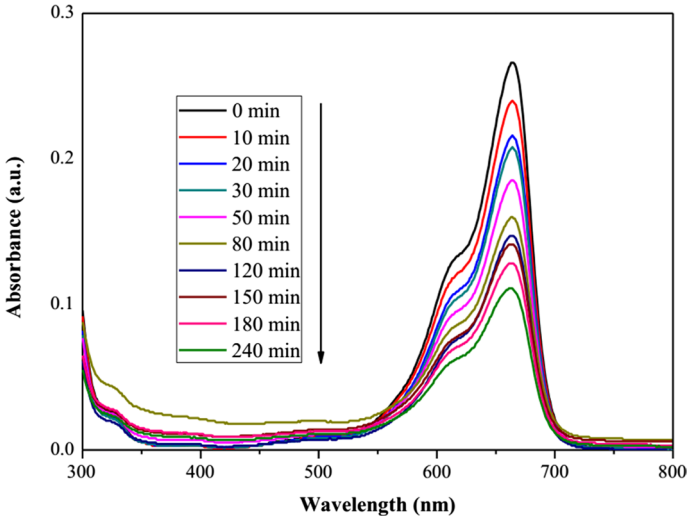

Fig. 7 Variation of UV–Vis absorption spectra of MB solution by SCT film at different time intervals (see "Photocatalytic studies" section for experimental conditions)

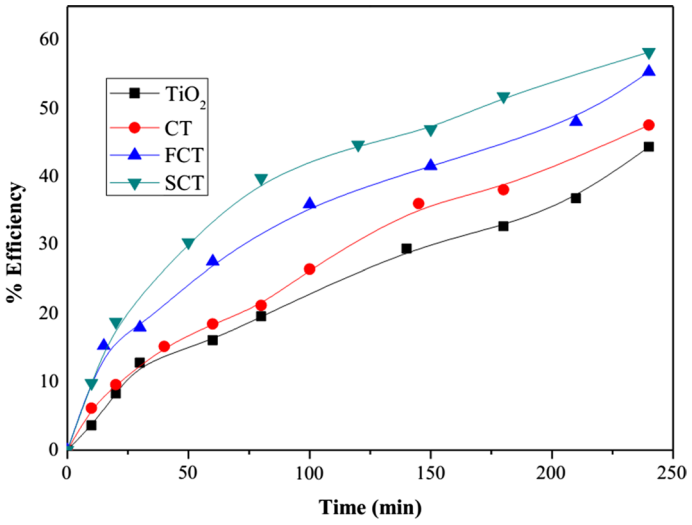

Fig. 8 Variation of photocatalytic degradation (% efficiency) of methylene blue dye over TiO_2, CT, FCT, and SCT films versus irradiation time (min)

disinfecting medical devices and in home appliances for water treatment. It is also reported that silver exerts an antibacterial function itself [32]. For our case, it can be assumed that Ag acted as an antibacterial agent as well as a dopant in the TiO_2

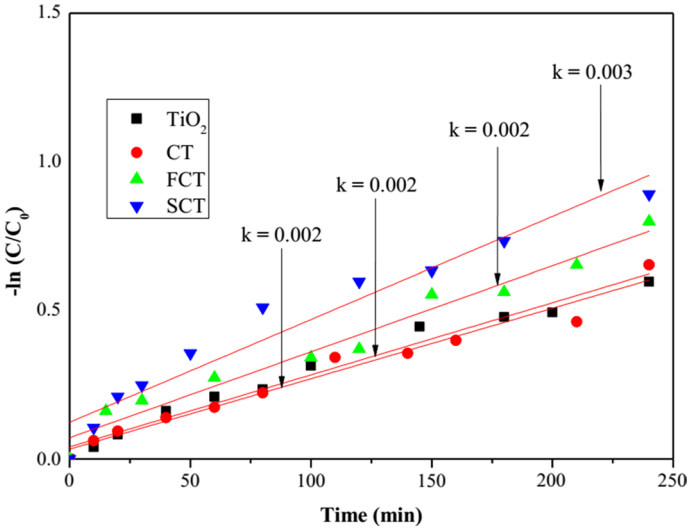

Fig. 9 Pseudo-first-order kinetics of degradation of methylene blue dye over TiO_2, CT, FCT, and SCT films versus irradiation time

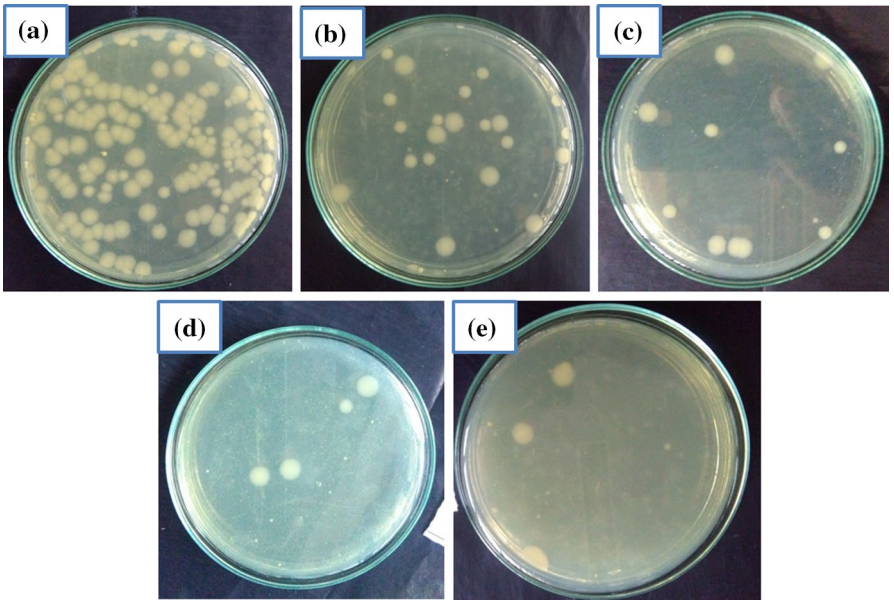

Fig. 10 Colony-forming units (CFUs) of *E. coli* after visible-light irradiation for 60 min: **a** without catalyst, and in presence of **b** bare-TiO_2, **c** CT, **d** FCT, and **e** SCT composite thin films

matrix. Our results indicate that the synthesized Ag–TiO_2–MWCNT composite film showed outstanding antimicrobial activity (Fig. 11).

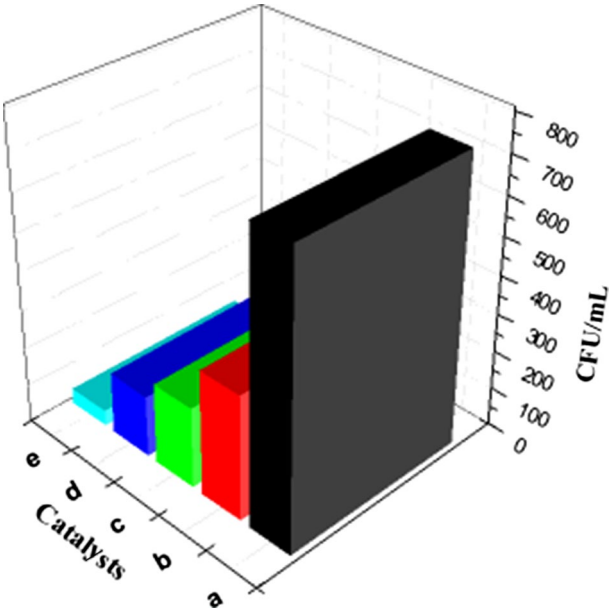

Fig. 11 Antibacterial efficiency: **a** without catalyst, and with **b** bare-TiO_2, **c** CT, **d** FCT, and **e** SCT thin films

These results reveal that the Ag–TiO_2–MWCNT nanocomposite could be used as an effective growth inhibitor of *E. coli*, representing a potential alternative to conventional chemicals for application as a stable photocatalyst in simultaneous wastewater treatment and disinfection for environmental protection.

Proposed degradation mechanism

The mechanism of the photocatalytic activity of the metal (Ag or Fe)-doped TiO_2–MWCNT photocatalysts is presented schematically in Fig. 12.

Illumination of pure TiO_2 with visible light causes excitation of electrons from the valence to conduction band, creating electron–hole pairs (e^-/h^+). In case of pure titania, only a small quantity of these e^-/h^+ pairs take part in the photocatalytic reaction due to their rapid recombination, resulting in lower activity for MB dye degradation. Incorporation of metals (Fe, Ag) and CNT in the TiO_2 matrix can prevent such rapid recombination of e^-/h^+ pairs, resulting in improved efficiency. The high degradation efficiency of the metal (Ag or Fe)-doped TiO_2/CNTs photocatalysts is attributed to the bandgap decrease on metal doping and high adsorption capacity of the CNT. These results show that the SCT nanocomposite thin film may show enhanced effects for MB degradation catalyzed by TiO_2 as well as adsorption of MB by CNTs. Based on the data presented above, the SCT composite thin film showed enhanced MB degradation compared with pure TiO_2, CT, or FCT under visible-light irradiation. This result suggests that doping Ag in TiO_2 with CNTs increased the

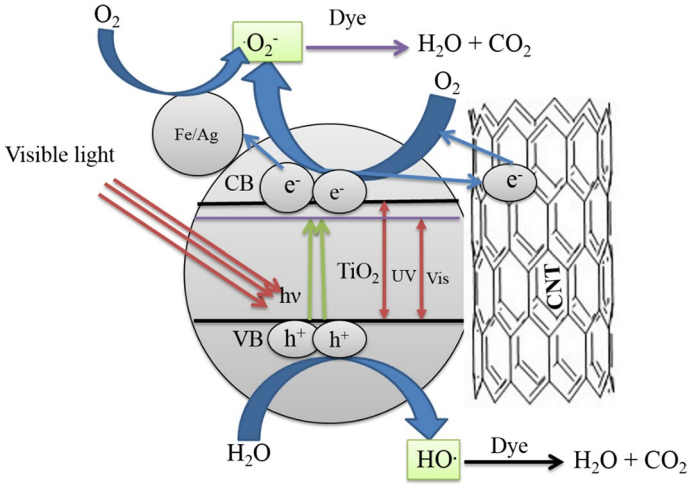

Fig. 12 Proposed photocatalysis mechanism of metal-doped TiO_2–MWCNT photocatalyst under visible-light irradiation

photocatalytic activity under visible-light irradiation, which can be ascribed to not only electron acceptance and good absorbance by CNTs, but also improved charge (e^-/h^+) separation via trapping of photoelectrons. This improved efficiency of the composites is in good agreement with results presented previously [33], where it was also mentioned that MWCNT can act as good electron acceptors under visible-light irradiation. In addition, the Ag and Fe dopants also act as electron-trapping materials by inhibiting e^-/h^+ pair recombination [34, 35].

Conclusions

New kinds of composite photocatalysts were successfully prepared by coupling MWCNT with silver- or iron-doped TiO_2 via a facile two-step sol–gel route at low temperature. The experimental results reveal dye degradation efficiency of 40.39, 47.66, 55.45, and 58.27 % for the TiO_2, CT, FCT, and SCT films, respectively, under visible-light irradiation for a maximum of 240 min. The SCT photocatalyst had smaller crystalline size and larger surface area than bare-TiO_2. A synergistic effect on the photocatalytic degradation of MB was observed for the SCT and FCT composite catalysts, which exhibited higher photocatalytic activity than CT or bare TiO_2. Therefore, addition of a suitable amount of MWCNT and silver or iron to TiO_2 can greatly improve its photocatalytic activity and expand the spectral response range to the visible-light region. In addition, SCT also clearly acted as a strong disinfectant for use in environmental protection applications.

Acknowledgements The authors would like to thank Dr. Erman Bengu of Bilkent University, Turkey for supply of CNTs and are also grateful to the World Academy of Sciences (TWAS), Department of

Chemistry, Shahjalal University of Science and Technology (SUST), University Research Center, SUST, University Grants Commission, Bangladesh, Ministry of Science and Technology, Bangladesh and Ministry of Education, Bangladesh for research grants to carry out this work.

References

1. N. Liu, X. Chen, J. Zhang, J.W. Schwank, Catal. Today **225**, 34 (2014)
2. P. Van Viet, B.T. Phan, D. Mott, S. Maenosono, T.T. Sang, C.M. Thi, L. Van Hieu, J. Photochem. Photobiol. A Chem. **352**, 106 (2018)
3. R. Hao, G. Wang, H. Tang, L. Sun, C. Xu, D. Han, Appl. Catal. B Environ. **187**, 47 (2016)
4. Z. Luo, A.S. Poyraz, C.H. Kuo, R. Miao, Y. Meng, S.Y. Chen, T. Jiang, C. Wenos, S.L. Suib, Chem. Mater. **27**, 6 (2015)
5. M.A. Ahmed, E.E. El-Katori, Z.H. Gharni, J. Alloys Compd. **553**, 19 (2013)
6. C.M. Lee, P. Palaniandy, I. Dahlan, Environ. Earth Sci. **76**, 611 (2017)
7. M.N. Uddin, S.U.A. Shibly, R. Ovali, S. Islam, M.M.R. Mazumder, M.S. Islam, M.J. Uddin, O. Gulseren, E. Bengu, J. Photochem. Photobiol. A Chem. **254**, 25 (2013)
8. M. Qamar, Q. Drmosh, M.I. Ahmed, M. Qamaruddin, Z.H. Yamani, Nanoscale Res. Lett. **10**, 54 (2015)
9. W. Mekprasart, T. Khumtong, J. Rattanarak, W. Techitdheera, W. Pecharapa, Energy Proc. **34**, 746 (2013)
10. S. Anandan, T. Narasinga Rao, M. Sathish, D. Rangappa, I. Honma, M. Miyauchi, ACS Appl. Mater. Interfaces **5**, 207 (2013)
11. B. Choudhury, A. Choudhury, J. Lumin. **132**, 178 (2012)
12. Z. Chen, L. Fang, W. Dong, F. Zheng, M. Shen, J. Wang, J. Mater. Chem. A **2**, 824 (2014)
13. K. Gopinath, S. Kumaraguru, K. Bhakyaraj, S. Thirumal, A. Arumugam, Superlattices Microstruct. **92**, 100 (2016)
14. B. Gao, T. Wang, X. Fan, H. Gong, H. Guo, W. Xia, Y. Feng, X. Huang, J. He, Inorg. Chem. Front. **4**, 898 (2017)
15. P. Sun, L. Liu, S.-C. Cui, J.-G. Liu, Catal. Lett. **144**, 2107 (2014)
16. S.M.H. AL-Jawad, A.A. Taha, M.M. Salim, Opt. Int. J. Light Electron. Opt. **142**, 42 (2017)
17. O. Akhavan, R. Azimirad, S. Safa, M.M. Larijani, J. Mater. Chem. **20**, 7386 (2010)
18. N. Abbas, G.N. Shao, M.S. Haider, S.M. Imran, S.S. Park, S.-J. Jeon, H.T. Kim, Mater. Sci. Eng. C **68**, 780 (2016)
19. B. Tryba, M. Piszcz, B. Grzmil, A. Pattek-Janczyk, A.W. Morawski, J. Hazard. Mater. **162**, 111 (2009)
20. Y.J. An, W.S. Chung, J. Chang, H.C. Lee, Y.R. Cho, Mater. Lett. **62**, 4277 (2008)
21. K.M. Rahulan, S. Ganesan, P. Aruna, Adv. Nat. Sci. Nanosci. Nanotechnol. **2**, 25012 (2011)
22. V. Vamathevan, R. Amal, D. Beydoun, G. Low, S. McEvoy, J. Photochem. Photobiol. A Chem. **148**, 233 (2002)
23. F. Zhang, M. Chen, W. Oh, New Carbon Mater. **25**, 348 (2010)
24. S. Wang, S. Zhou, J. Hazard. Mater. **185**, 77 (2011)
25. M.J. Uddin, M.M. Alam, M.A. Islam, S.R. Snigda, S. Das, M.M. Rahman, M.N. Uddin, C.A. Morris, R.D. Gonzalez, U. Diebold, T.J. Dickens, O.I. Okoli, Int. Nano Lett. **3**, 16 (2013)
26. M.N. Uddin, M.S. Islam, M.M.R. Mazumder, M.A. Hossain, M. Elias, I.A. Siddiquey, M.A.B.H. Susan, D.K. Saha, M.M. Rahman, A.M. Asiri, S. Hayami, J. Incl. Phenom. Macrocycl. Chem. **82**, 229 (2015)
27. Y. Xie, C. Yuan, Appl. Catal. B Environ. **46**, 251 (2003)
28. A.V. Vinogradov, A.V. Agafonov, V.V. Vinogradov, O.I. Davydova, Mendeleev Commun. **22**, 27 (2012)
29. L.M. Santos, W.A. Machado, M.D. Franca, K.A. Borges, R.M. Paniago, A.O.T. Patrocinio, A.E.H. Machado, RSC Adv. **5**, 103752 (2015)
30. N. Nasralla, M. Yeganeh, Y. Astuti, S. Piticharoenphun, N. Shahtahmasebi, A. Kompany, M. Karimipour, B.G. Mendis, N.R.J. Poolton, L. Šiller, Sci. Iran. **20**, 1018 (2013)
31. P.C. Maness, S. Smolinski, D.M. Blake, Z. Huang, E.J. Wolfrum, W.A. Jacoby, Appl. Environ. Microbiol. **65**, 4094 (1999)

32. V. Sambhy, M.M. MacBride, B.R. Peterson, A. Sen, J. Am. Chem. Soc. **128**, 9798 (2006)
33. M. Chen, F. Zhang, W. Oh, New Carbon Mater. **24**, 159 (2009)
34. N. Sobana, M. Muruganadham, M. Swaminathan, J. Mol. Catal. A Chem. **258**, 124 (2006)
35. X. Yang, C. Cao, L. Erickson, K. Hohn, R. Maghirang, K. Klabunde, Appl. Catal. B Environ. **91**, 657 (2009)